Point-process models of social network interactions: parameter estimation and missing data recovery

JOSEPH R. ZIPKIN[1], FREDERIC P. SCHOENBERG[2], KATHRYN CORONGES[3], and ANDREA L. BERTOZZI[4]

[1] *Department of Mathematics, University of California, Los Angeles, Los Angeles, CA 90095, USA*
email: zipkinj@acm.org
[2] *Department of Statistics, University of California, Los Angeles, Los Angeles, CA 90095, USA*
[3] *Department of Behavioral Sciences and Leadership, United States Military Academy, West Point, NY 10996, USA*
[4] *Department of Mathematics, University of California, Los Angeles, Los Angeles, CA 90095, USA*

(*Received August 24, 2015*)

Electronic communications, as well as other categories of interactions within social networks, exhibit bursts of activity localised in time. We adopt a self-exciting Hawkes process model for this behaviour. First we investigate parameter estimation of such processes and find that, in the parameter regime we encounter, the choice of triggering function is not as important as getting the correct parameters once a choice is made. Then we present a relaxed maximum likelihood method for filling in missing data in records of communications in social networks. Our optimisation algorithm adapts a recent curvilinear search method to handle inequality constraints and a nonvanishing derivative. Finally we demonstrate the method using a data set composed of email records from a social network based at the United States Military Academy. The method performs differently on this data and data from simulations, but the performance degrades only slightly as more information is removed. The ability to fill in large blocks of missing social network data has implications for security, surveillance, and privacy.

1 Introduction

1.1 Burstiness and Hawkes processes

The ways humans interact has long been a subject of interest. The rise of electronic communication, and particularly social media, has made large data sets of human interactions available. Growing interest in privacy and cybercommunications has led to questions about what can be learned from this data and how it is used.

A natural first question is how to model patterns of social interactions. A point process seems a natural choice, but the simplest point process, the Poisson process, is ill suited to modeling several classes of human activity, including communication. The problem, broadly speaking, is that human activity patterns tend to be "bursty", that is, more tightly clustered in time than a Poisson process. See, for example, Figure 1. Two point patterns are plotted. Figure 1(a) is taken from the IkeNet data set, which will be dis-

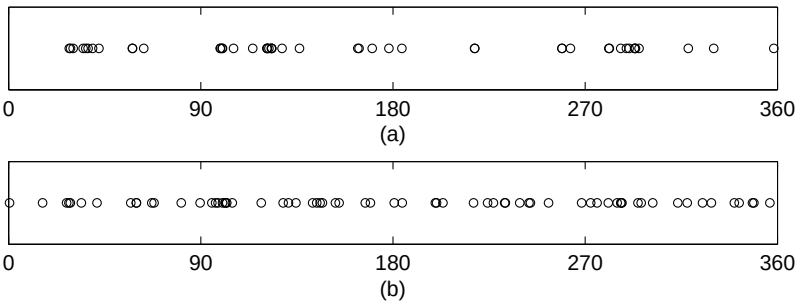

FIGURE 1. Two point patterns. The axis is time in days, and circles indicate events. Each point pattern has 68 events. (a) Timestamps of emails sent between IkeNet user 6 and IkeNet user 15. (b) A simulated Poisson process.

cussed in detail later. It shows the times that two particular users sent each other emails. Figure 1(b) is a realisation of a Poisson process. The two point patterns have the same number of events, but the IkeNet point pattern is more strongly clustered. This suggests a Poisson process is a suboptimal choice for modelling human interactions. Furthermore, the absence of any apparent time scale of usual periodic human behavior (hourly, daily, weekly, even monthly) rules out a non-homogeneous Poisson process with deterministic intensity. Bursty dynamics have been observed in Web browsing [35], emails [1], communications within electronic social networking systems [33], mobile phone calls [24], FTP requests [30], and even face-to-face interactions [16].

In 1971 Hawkes [13, 14] introduced a class of *self-exciting point processes* that have come to bear his name. A *Hawkes process* is a nonhomogeneous point process $n(t)$ whose intensity is governed by

$$\lambda(t) = \mu + \sum_{t_i<t} g(t - t_i; \theta). \tag{1.1}$$

Each t_i is an event time, μ is a deterministic *background intensity*, and g is a *triggering function* specifying how much a recent event increases the intensity, hence the notion of the Hawkes process as self-exciting. Here we note explicitly the dependence of g on a vector θ of parameters because we will estimate these parameters statistically, but we may omit it later for notational convenience. (Nonparametric approaches to estimating g have also been developed [18, 21].) Likewise we may write $\lambda(t|\{t_i\}_{i=1}^{n(t)})$ when we want to emphasise the dependence of λ on the history. The background intensity μ can be time-dependent, but we take it as a constant for simplicity. This choice has precedent in seismology [21].

Figure 2 shows Hawkes process realisations with $\mu = 0.15$ and $g(t) = 0.5e^{-0.6t}$. The intensity and event times are plotted against time. The Hawkes process events are more tightly clustered in time than the Poisson process of Figure 1(b), perhaps more closely resembling Figure 1(a).

The Hawkes process appears in the seismology literature as a model for the timing of earthquakes and their aftershocks [26]. As interest in and availability of large data sets of human activities have grown, Hawkes processes have been used to model electronic

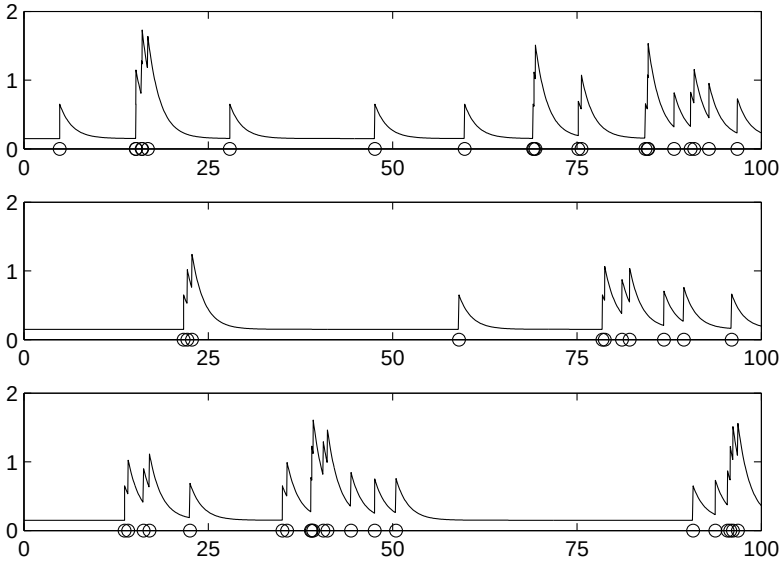

FIGURE 2. Three realisations of a Hawkes process with $\mu = 0.15$ and $g(t) = 0.5e^{-0.6t}$. The horizontal axis is time. Circles indicate events, and the solid curve is the intensity.

communications [5], gang crimes [10, 15, 34], and even terrorist and insurgent activity [19, 25].

The constraints on μ and g are modest. First, we assume that $\mu > 0$. Second, so that the process is self-exciting rather than self-dampening, we assume g is non-negative. Finally, we assume that $\int_0^\infty g(t;\theta)dt < 1$ to ensure that the process is stationary. The importance of this assumption becomes clear when we recognise that $\int_0^\infty g(t;\theta)dt$ is the expected number of immediate descendants of each event. Were it greater than 1, then each event could be expected to give rise to infinitely many others. This would make the process explosive and impossible to simulate repeatedly. It also runs against intuition for our application to emails within a social network (all email threads end eventually) or indeed any of the other applications mentioned above.

Our approach recalls that of Stomakhin, Short & Bertozzi's work on networks of criminal gang rivalries [34]. A gang that has been victimised by a rival will often retaliate, setting off a burst of tit-for-tat crimes. Stomakhin, Short & Bertozzi associate to each pair of rival gangs an independent Hawkes process whose events represent crimes committed by one gang against the other. Then, noting that law enforcement often knows which gang was victimised but not which gang was the perpetrator, they cast the task of solving the crime as a missing data problem, in which a history of gang crimes is known but some of the identities of the gangs involved in particular incidents are hidden. Like Stomakhin, Short & Bertozzi, we will assign independent Hawkes processes to the connections within a social network and solve a missing data problem. However, our variational approach will be different.

Lee *et al.* [17] also use message data to solve an inverse problem. However, they seek

Table 1. *Pairs of officers who exchanged* > 100 *emails*

Pair	Number of emails	Pair	Number of emails
(9,18)	1,042	(18,22)	222
(11,22)	511	(4,13)	134
(13,17)	302	(9,13)	131
(11,13)	293	(13,18)	130
(8,18)	281	(13,22)	120
(13,15)	223	(3,17)	116

the actors' positions in physical space rather than their identities. Also their approach is fundamentally Bayesian, while ours is based in maximum likelihood.

1.2 The IkeNet data set

Between 2010 and 2011, email exchange data was collected from 22 volunteers, all mid-career United States Army officers enrolled in the Eisenhower Leadership Development Program, a one-year graduate program administered jointly by Columbia University and the United States Military Academy. During their enrollment, members of this "Ike" network were given cell phones with which they could access their military email accounts. Of the 22 participants, 19 (90%) were male, and 17 (77%) were Caucasian. At the start of the project they ranged in age from 26 to 33 years.

The data set consists of time stamps and anonymised sender and receiver codes from 8,896 emails sent among the participating officers over a 361-day period. This is a social network with 253 connections. (We include self-connections because the volunteers emailed themselves.) Emails were sent along 250 of these connections.

The emails are by no means distributed evenly among these 250 connections. Table 1 lists the 12 pairs of officers who exchanged more than 100 emails. The top pair (9,18) exchanged 1,042 emails, or 11.7% of all the emails in the corpus. Together these top 12 exchanged 3,505 emails, or 39.4% of the corpus. Figure 3 is a histogram of the number of emails exchanged among the remaining pairs, all of them less than 100. Many of the pairs of officers exchanged only a few emails, while a few pairs exchanged a substantial proportion of all emails in the corpus, and a few users (13, 18, 22) appear three times or more in this list of highly active pairs. These observations are consistent with a core–periphery structure, which is a characteristic of many social networks [7].

Fox *et al.* [11] perform several statistical studies of this data set, including fitting Hawkes processes to the email patterns via maximum likelihood estimation. They find that a Hawkes process model fits the IkeNet data better than a homogeneous Poisson model, as measured by the Akaike information criterion (AIC). They also incorporate the results of a leadership survey administered to the volunteers, revealing more details of the social network.

Our approach differs from Fox *et al.*'s in two basic ways. First, while they assign an independent Hawkes process to each officer (i.e., each node in the network), we assign one to each relationship between officers (i.e., each edge in the network). This is appropriate

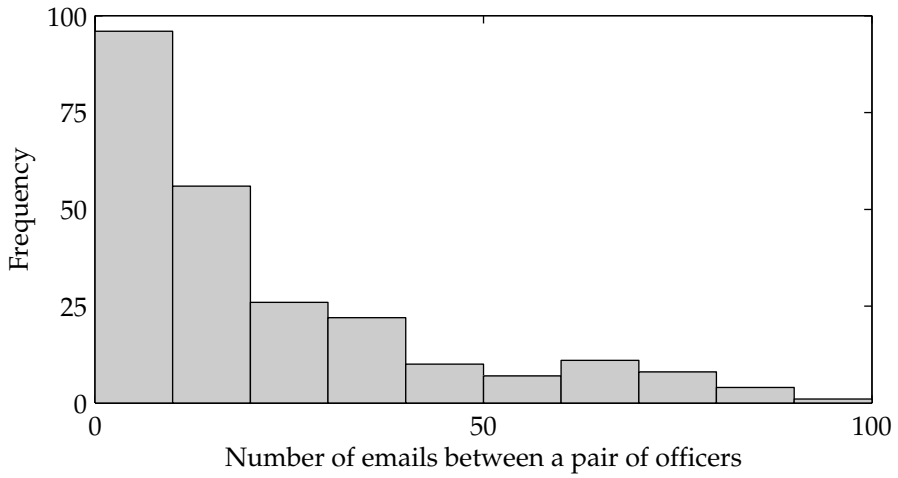

FIGURE 3. Histogram of the number of emails sent between each pair of officers. Only pairs who exchanged fewer than 100 emails are shown; see Table 1 for the others.

to the missing data problem, in which differences in the officers' relationships matter a great deal. Second, while Fox *et al.* allow the background rate μ to change periodically to capture daily and weekly rhythms in email traffic, we take μ as a constant. We expect this simplification's impact to be modest, because Fox *et al.* found only a modest improvement in AIC by moving to a time-varying μ, and because we do not expect it to have much import for our missing data problem.

2 EM estimation of Hawkes process parameters

First we must discuss fitting the parameters of a Hawkes process to data. We take a maximum-likelihood approach, using an expectation-maximisation numerical method to combat the problem's ill conditioning [36]. Finally, we give several examples for different choices of the triggering function g. It is most common in the literature to assume an exponential form for g [5, 11, 15, 22, 34], though other forms are also in use, including power law [6, 27] and the exponential multiplied by a polynomial [28]. Our comparison of exponential and power-law forms suggests that it does not matter which is used, validating the frequent use of the exponential form.

The general problem is, given an interval $[0, T]$ and a point pattern $\{t_i\}_{i=1}^{n(T)}$ falling in that interval, to produce statistical estimates $\hat{\mu}$ and $\hat{g}$ for the μ and g of the Hawkes process assumed to generate the data. Nonparametric methods of estimating g exist [18], but our approach will be to assume a form for g (in statistical parlance, to adopt a *model* for g) and instead estimate θ, the vector of parameters, together with μ using maximum likelihood, yielding parameter estimates $(\hat{\mu}, \hat{\theta})$.

The likelihood that a point process with conditional intensity λ generated a history

$\{t_i\}_{i=1}^{n(T)}$ is

$$L = \exp\left(-\int_0^T \lambda(t|\{t_i\}_{i=1}^{n(T)})dt \right) \prod_{i=1}^{n(T)} \lambda(t_i|\{t_j\}_{j=1}^{i-1}). \tag{2.1}$$

See [31] for a detailed discussion. It is standard to instead maximise the log-likelihood, which for a Hawkes process as in (1.1) has the form

$$\log L(\mu, \theta) = \sum_{i=1}^{n(T)} \left(\log\left(\mu + \sum_{j=1}^{i-1} g(t_i - t_j; \theta) \right) - \int_0^{T-t_i} g(t; \theta)dt \right) - \mu T. \tag{2.2}$$

Ozaki [29] treats maximum likelihood estimation of the parameters when g is exponential.

2.1 Generating Hawkes process point patterns

Throughout this section, and again in section 4 when considering simulated networks, we use Lewis's thinning method [20, 26] to generate artificial Hawkes process point patterns. Briefly, given a history $\{t_i\}_{i=1}^n$ at time t, we simulate an independent exponential random variable s with rate parameter $\lambda(t|\{t_i\}_{i=1}^n)$. Were this process homogeneous, we would take $t_{n+1} = t + s$, set $t = t + s$, and continue. However, because the intensity decays following an event, we only do this with probability $\lambda(t + s|\{t_i\}_{i=1}^n)/\lambda(t|\{t_i\}_{i=1}^n)$. If we do not, we set $t = t + s$ and generate a new s. The procedure continues until $t > T$.

2.2 The EM algorithm

Fox *et al.* [11] use the standard optimisation routines in the R software package to estimate the parameters of a Hawkes process model by likelihood maximisation. However, they model each *agent* as an independent Hawkes process, where we assign an independent Hawkes process to each *relationship between the agents*. If we conceive of the IkeNet social network as a graph, Fox *et al.* model the nodes, and we model the edges. This places us in different parameter regimes where the conditioning may be different.

The condition number of maximising the smooth log-likelihood is

$$\kappa = \frac{\|\nabla^2 \log L(\hat{\mu}, \hat{\theta})\| \|(\hat{\mu}, \hat{\theta})\|}{\|\nabla \log L(\hat{\mu}, \hat{\theta})\|},$$

where ∇^2 denotes the Hessian and $\hat{\mu}$ and $\hat{\theta}$ are the values of μ and θ maximising $L(\mu, \theta)$. (The notation does not show it explicitly, but κ also depends on T.) To demonstrate the condition numbers we can expect to encounter in this work, we generated 50,000 realisations of a Hawkes process with the exponential triggering function $g(t; \theta) = g(t; \alpha, \omega) = \alpha\omega e^{-\omega t}$, taking $T = 361$, $\mu = 0.05$, $\alpha = 0.5$, and $\omega = 6$. (These values were chosen to correspond with a typical edge in the IkeNet data.) We then used the EM algorithm described below to compute $\hat{\mu}$ and $\hat{\theta} = (\hat{\alpha}, \hat{\omega})$ for each realisation. The condition numbers varied widely, but 95% of them fell in the interval $(2.7 \times 10^5, 1.4 \times 10^9)$. These are very high condition numbers, indicating that standard iterative methods may converge unacceptably slowly for this problem.

Veen & Schoenberg [36] show how to use an expectation-maximisation (EM) algorithm

to counter the problem's ill conditioning. The algorithm relies on the Hawkes process's branching structure. The linearity of the conditional intensity process (1.1) allows us to calculate the probability that a given event was triggered by any previous event; otherwise it is a *background* event. The probability that an event occurring at time t_i is a background event is $\mu/\lambda(t_i)$, and the probability that it was caused by an event that occurred at time $t_j < t_i$ is $g(t_i - t_j)/\lambda(t_i)$.

The EM algorithm alternates between an *expectation step* and a *maximisation step*. At the k^{th} iteration we have an estimate $(\mu^{(k)}, \theta^{(k)})$ of the parameters. The expectation step of the $(k+1)^{\text{th}}$ iteration uses those parameters to calculate $p_{i,i}^{(k+1)}$ and $p_{i,j}^{(k+1)}$, respectively the probabilities that event i was a background event or was caused by event j:

$$p_{i,i}^{(k+1)} = \frac{\mu^{(k)}}{\mu^{(k)} + \sum_{j=1}^{i-1} g(t_i - t_j; \theta^{(k)})},$$
$$p_{i,j}^{(k+1)} = \frac{g(t_i - t_j; \theta^{(k)})}{\mu^{(k)} + \sum_{j=1}^{i-1} g(t_i - t_j; \theta^{(k)})}.$$

The maximisation step targets *complete data likelihood* of the branching structure. The likelihood of a given structure can be decomposed into independent pieces:

- The number of background events. This is a Poisson random variable (call it b) with expectation μT. Its likelihood is
$$L_1(\mu) = e^{-\mu T} \frac{(\mu T)^b}{b!}.$$
- The number of immediate descendants of each event, both background and triggered, given b. Let d_i be the number of descendants of event i. It is also Poisson, and its expectation is $\int_0^{T-t_i} g(t;\theta)dt$. Lewis & Mohler [18] found that approximating this by $G(\theta) = \int_0^{\infty} g(t;\theta)dt$ had only a modest impact on the reliability of results, so we adopt this approximation for simplicity. Because each d_i is independent of the others, their joint likelihood is
$$L_2(\theta) = \prod_{i=1}^{n} e^{-G(\theta)} \frac{G(\theta)^{d_i}}{d_i!}.$$
- The timing of the descendant events given b and all the d_i. Let $j(i)$ be the event of which i is the immediate descendant, with $j(i) = i$ if i is a background event. The likelihood of event i occurring at time t_i is $g(t_i - t_{j(i)};\theta)/G(\theta)$ (we again approximate a finite integral of g by $G(\theta)$), so the joint likelihood of all events' timing is
$$L_3(\theta) = \prod_{i:j(i)<i} \frac{g(t_i - t_{j(i)};\theta)}{G(\theta)}.$$
The background events are distributed uniformly in $[0, T]$, so their timing does not enter into the likelihood.

The likelihood of the overall branching structure is the product of $L_1(\theta)$, $L_2(\theta)$, and $L_3(\theta)$. The maximisation step is sometimes said to maximise this likelihood. In fact, it maximises the expectation of the log-likelihood under the probability measure implied by the $p^{(k+1)}$ computed in the expectation step [23, pp. 18–20]. This suffices to maximise

the likelihood over the course of the algorithm [39]. The log-likelihood is

$$\ell_c(\mu,\theta) = -\mu T + b\log\mu + b\log T - \log(b!) + \sum_{i=1}^{n}(-G(\theta) + d_i \log G(\theta) - \log(d_i!)) + \sum_{i:j(i)<i} (\log g(t_i - t_{j(i)};\theta) - \log G(\theta)).$$

The parameters (μ,θ) are exogenous to the probability measure implied by the $p^{(k+1)}$, so additive terms that do not depend explicitly on (μ,θ) are constants under expectation. Thus it is equivalent to maximise the function

$$E^{(k+1)}(\mu,\theta) = -\mu T + (\log\mu)\sum_{i=1}^{n} p_{i,i}^{(k+1)} - nG(\theta) + \sum_{i=1}^{n}\sum_{j=1}^{i-1} p_{i,j}^{(k+1)} \log g(t_i - t_j;\theta).$$

Regardless of the model for g, the maximising value of μ is

$$\hat{\mu}^{(k+1)} = \frac{\sum_{i=1}^{n} p_{i,i}^{(k+1)}}{T}.$$

The maximising θ satisfies

$$\nabla G(\hat{\theta}^{(k+1)}) = \frac{1}{n}\sum_{i=1}^{n}\sum_{j=1}^{i-1} p_{i,j}^{(k+1)} \frac{\nabla_\theta g(t_i - t_j;\hat{\theta}^{(k+1)})}{g(t_i - t_j;\hat{\theta}^{(k+1)})}. \tag{2.3}$$

Fortunately, for both the models we choose for g, (2.3) reduces to tractable algebraic expressions for each component of $\hat{\theta}^{(k+1)}$.

2.3 Example: exponential triggering

First, we choose $g(t;\alpha,\omega) = \alpha\omega e^{-\omega t}$. The L^1 condition on g is equivalent to $\omega > 0$ and $0 \le \alpha < 1$. The θ condition (2.3) reduces to

$$\hat{\alpha}^{(k+1)} = \frac{\sum_{i=1}^{n}\sum_{j=1}^{i-1} p_{i,j}^{(k)}}{n}, \qquad \hat{\omega}^{(k+1)} = \frac{\sum_{i=1}^{n}\sum_{j=1}^{i-1} p_{i,j}^{(k)}}{\sum_{i=1}^{n}\sum_{j=1}^{i-1} p_{i,j}^{(k)}(t_i - t_j)}.$$

We generated 50,000 realisations of a Hawkes process with this triggering function, taking $T = 361$, $\mu = 0.05$, $\alpha = 0.5$, and $\omega = 6$ as in Section 2.2. We then estimated the parameters using the EM algorithm. The results are presented in Table 2 and Figure 4(a). The estimates for the parameters are distributed about their ground-truth values, with a slight rightward skew for μ and more pronounced leftward and rightward skews for α and ω, respectively. Of the 50,000 estimates for ω, 504 or about 1% were greater than 18; these are omitted from the histogram.

Given the opposite skews of μ and α and the roles they play in the formula for the conditional intensity, one may be tempted to speculate that underestimates of μ are associated with overestimates of α, and vice-versa. We find that the sample values of μ and α have a real but weak relationship: they have a slightly negative Spearman rank correlation ($\rho = -9.46 \times 10^{-3}$, $p = 0.034$). The Pearson correlation is $r = 2.65 \times 10^{-3}$ ($p = 0.554$), so this relationship is likely nonlinear.

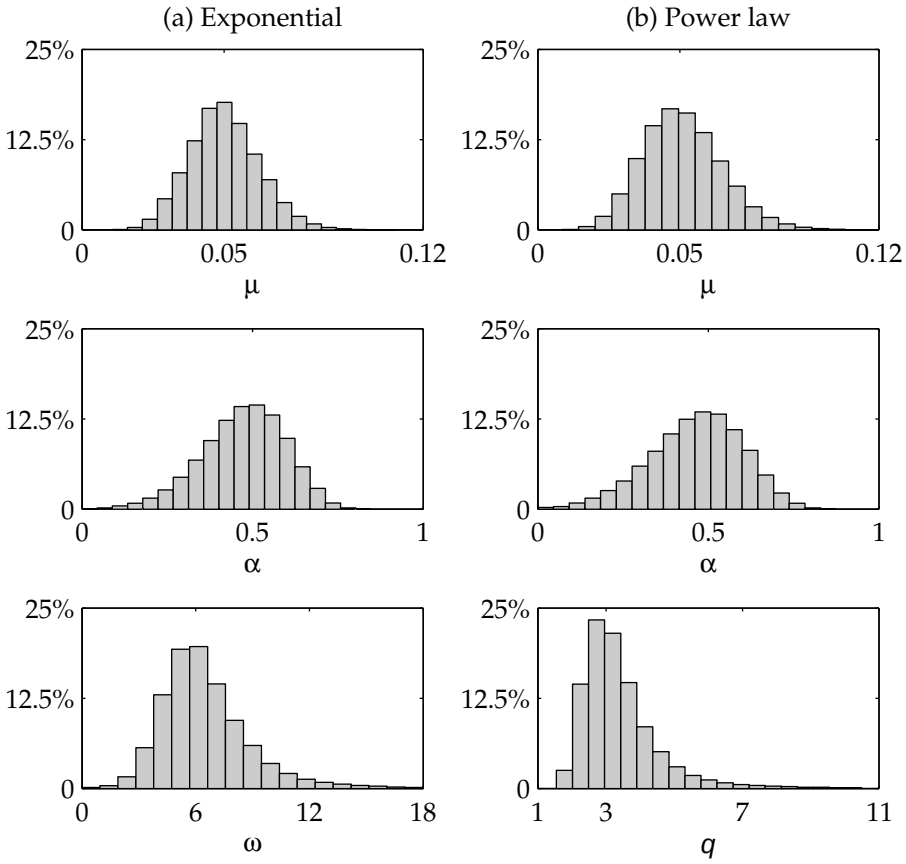

FIGURE 4. Histograms showing the results of EM estimation of model parameters for (a) exponential and (b) power law triggering functions. For each model 50,000 point patterns were generated. About 1% of the results for ω and q are omitted because they are outliers that exceed the right limit of the graph.

Table 2. *EM estimation results*

Model	Parameter	Ground truth	Mean
Exponential	μ	0.05	0.05002
	α	0.5	0.4733
	ω	6	6.753
Power law	μ	0.05	0.05095
	α	0.5	0.4641
	q	3	3.590

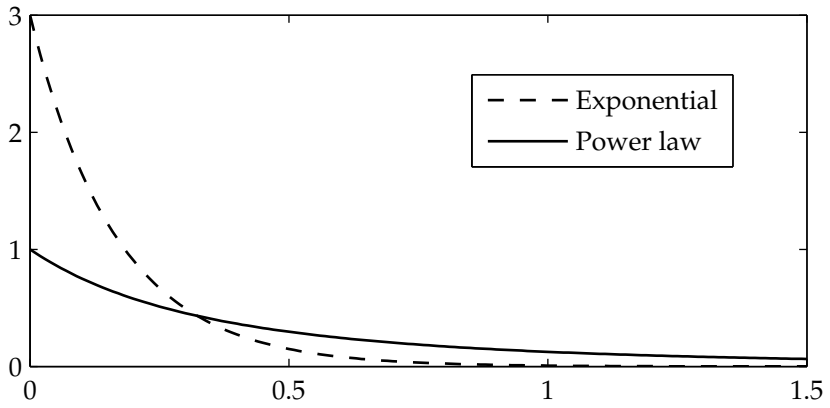

FIGURE 5. Triggering functions. Exponential: $g(t) = 3e^{-6t}$. Power law: $g(t) = (1+t)^{-3}$.

2.4 Example: power-law triggering

Many human behaviour patterns exhibit power-law scaling in inter-event times [1]. Therefore, we now choose $g(t;\alpha,q) = \alpha(q-1)(1+t)^{-q}$. This has the same number of parameters as the previous section's exponential model. The L^1 condition on g is equivalent to $q > 1$ and $0 \le \alpha < 1$. The θ condition (2.3) reduces to

$$\hat{\alpha}^{(k+1)} = \frac{\sum_{i=1}^{n}\sum_{j=1}^{i-1} p_{i,j}^{(k)}}{n}, \qquad \hat{q}^{(k+1)} = 1 + \frac{\sum_{i=1}^{n}\sum_{j=1}^{i-1} p_{i,j}^{(k)}}{\sum_{i=1}^{n}\sum_{j=1}^{i-1} p_{i,j}^{(k)} \log(1+t_i-t_j)}.$$

Again, we generated 50,000 realisations with T, μ, and α as above, and $q = 3$. The results are presented in Table 2 and Figure 4(b). As with the exponential triggering function, estimates for μ and α are overall close to their ground truths with, respectively, a slight rightward skew and a more pronounced leftward skew,. The estimates of q clearly peak around 3 but skew rightward. Of the 50,000 estimates for q, 446 or about 0.9% were greater than 11; these are omitted from the histogram.

2.5 Comparison of exponential and power-law

In practice we may not know the best form of the triggering function to use when modelling a point process. Nonparametric methods are one solution [18]; however, these can be cumbersome, and without enough data they invite overfitting. Instead we ask whether point patterns generated by the two triggering functions discussed in sections 2.3 and 2.4 can be told apart. The triggering functions are plotted together in Figure 5. They have the same integral, but the power-law triggering function has a longer tail. One might reasonably expect these two triggering functions to produce different behaviours.

Most of the time we consider the likelihood only in the context of maximising it with respect to the parameters or the model, given a history. But the likelihood has comparative value, as well. Comparing the likelihoods of models or sets of parameters to the maximum likelihood value reveals how much likelihood we lose by adopting suboptimal assumptions.

Table 3. *Mean log-loss vs. correct EM, fit and validated on same dataset*

Model Parameters	Correct EM	Incorrect EM	Correct Ground truth	Incorrect "Ground truth"
Exponential	0	−0.11	−1.51	−7.47
Power-law	0	−0.05	−1.50	−7.66

Table 4. *Percent of Monte Carlo trials in Table 3 in which correct ground truth outperformed the given choice of model and parameters*

Model Parameters	Correct EM	Incorrect EM	Correct Ground truth	Incorrect "Ground truth"
Exponential	0.0%	13.1%	–	99.6%
Power-law	0.0%	24.0%	–	99.6%

To wit, we calculate different likelihood values given the 50,000 Hawkes process realisations we generated for each triggering function in sections 2.3 and 2.4. For each exponential history $H = \{t_i\}_{i=1}^n$, we compute the log-likelihood (2.2) of the EM parameters $(\hat{\mu}_{\exp}(H), \hat{\theta}_{\exp}(H))$ and the exponential ground-truth parameters $(0.05, 0.5, 6)$. We also calculate $(\hat{\mu}_{\text{pow}}(H), \hat{\theta}_{\text{pow}}(H))$, the parameters maximising the likelihood under a power law model, and compute their likelihood. For comparison we also compute the likelihood for the power-law ground-truth parameters $(0.05, 0.5, 3)$. We then repeat the process *mutatis mutandis* for each power-law history. In this way we hope to quantify the loss incurred by using the "wrong" model for the triggering function, as compared to the loss incurred by using the "right" model with the "wrong" parameters. Because both models have the same number of parameters, the penalty term of the Akaike information criterion is unnecessary.

Table 3 summarises the results. The rows indicate whether we used the exponential or power-law histories. Each column corresponds to a choice of model and a choice of parameters with which to equip it. Each entry is the average difference across all realisations in log-likelihood ("log-loss") between its column's given model–parameter combination and the "correct" model equipped with the EM parameters. The combination in the first column is the "correct" model and the EM parameters; the entries are zero by construction. The second column adopts the "incorrect" model but uses the likelihood-maximising parameters given that model. The third column uses the "correct" model's ground-truth parameters rather than the likelihood-maximising parameters. The fourth column uses the "incorrect" model's ground-truth parameters. We have no reason to expect this last category to perform well; we include it for a sense of scaling.

In both cases, the loss from using the EM parameters assuming the wrong model is substantially less than the loss from using the right model with the ground-truth parameters. To emphasise, these are the parameters *that actually generated the histories*, yet they do not fit the data as well as a certain set of parameters attached to the wrong model (though not every set, as the fourth column makes clear). The clear moral is

Table 5. *Mean log-loss vs. correct ground truth, fit and validated on different datasets*

Model Parameters	Correct EM	Incorrect EM	Correct Ground truth	Incorrect "Ground truth"
Exponential	−2.04	−2.01	0	−5.93
Power-law	−1.95	−2.53	0	−6.13

Table 6. *Percent of Monte Carlo trials in Table 5 in which correct ground truth outperformed the given choice of model and parameters*

Model Parameters	Correct EM	Incorrect EM	Correct Ground truth	Incorrect "Ground truth"
Exponential	53.3%	53.3%	–	60.9%
Power-law	76.8%	79.8%	–	93.9%

that, when maximising likelihood to fit Hawkes process models to data in our particular parameter regimes, selecting the "correct" model is not as important as finding the likelihood-maximising parameters once a model has been selected. More study is needed to discover how far this moral applies outside this specific context.

Finally, we note that this analysis is conducted with maximum-likelihood parameters applied to the same point pattern used to estimate the parameters. If the parameter estimation is performed on one point pattern and the results are assessed using another, separate realisation of the same point process, then the correct model with ground truth parameters will of course on average outperform the incorrect model or the correct model with fitted parameters. To illustrate, we generated 100,000 point patterns and randomly divided them into 50,000 training sets and 50,000 testing datasets. Each training sample was randomly paired with a testing sample, and the log-likelihood on the test sample was calculated using both ground-truth parameters and maximum-likelihood parameters trained on the corresponding training sample. Table 5 shows the results of this Monte Carlo experiment; the values are mean log-losses relative to the log-likelihood of the correct model with ground truth parameters. The results make clear that the improvement in log-likelihood obtained by fitting the parameters by MLE does not apply to external datasets but only to the dataset on which the fitting was performed. In what follows, when our methods are applied to the IkeNet point patterns, we may conclude that the fitted exponential triggering function offers sufficiently good fit to this dataset, though this of course would not necessarily imply satisfactory fit to other datasets obtained in the future.

3 The missing data problem

In this section we state the missing data problem and discuss its numerical solution. We take a variational approach, maximising a discriminant function subject to certain constraints. For the numerics we adapt the curvilinear method of Wen & Yin [38].

3.1 Objective functions

Suppose that we have records of N emails sent among a social network of V members, as in the IkeNet data set. But suppose that for some subset of the emails, we do not know who sent or received them. More generally, we want to identify which of the M edges each email in the subset was drawn from. Because M scales with V^2, a direct approach enumerating all possibilities and checking them is not scaleable. Instead, we relax the problem as in [34].

Number the M connections from 1 to M. (The order does not matter.) The history of events is $H = \{t_i\}_{i=1}^{N}$. This history is partitioned into C, the events for which we know which connection the event happened on, and I, the incomplete-information event. The complete set has the obvious partition $C = \bigcup_{m=1}^{M} C_m$ into the histories associated to each connection.

We present four methods for classifying the incomplete events. The first two are simple, model-free methods based on basic statistics of H. The other two are variational methods maximising a sort of score function. In each case we have what amounts to a family of discriminant functions, one for each of the M connections. The value of the discriminant function for $t_i \in I$ on connection m is $x_{i,m}$. We speak of x_i as the vector of weights associated to $t_i \in I$. Not every x_i need belong to the same space, or even have the same dimension, as the others. We need define $x_{i,m}$ only for those edges m to which t_i could belong. For example, if we know that one of the parties to an email was officer 1, we need not consider the weight on the connection between officers 2 and 3.

The first classification method is a *method of modes*, which sets $x_{i,m} = |C_m|$. The only dependence on i comes from the fact that we do not set $x_{i,m}$ if message i could not have been sent on connection m. The second method is a nearest-neighbor weighting, which weights depending on the proximity in time (forward or backward) of the nearest known event: $x_{i,m} = \max\{|t_i - t_j|^{-1} : t_j \in C_m\}$.[1] These two methods are in a sense dual to one another: the method of modes is a simple, model-free, global method, and the nearest-neighbor method is a simple, model-free, local method. They can serve as benchmarks for the other methods, which assume a Hawkes process model and in so doing incorporate both global and local information.

The third method for $x_{i,m}$ is a relaxed maximum likelihood method. The likelihood of a given history and parameter set is

$$L = \left(\prod_{t_i \in I} \lambda_{m_i}(t_i) \right) \prod_{m=1}^{M} \left(\prod_{t_i \in C_m} \lambda_m(t_i) \right) e^{-\int_0^T \lambda_m(t)dt}.$$

A true MLE approach would find the $\{m_i : t_i \in I\}$ maximising the likelihood. However, there are $M^{|I|}$ possible values, so this approach quickly becomes infeasible as M and $|I|$ grow. We instead consider a relaxed problem, in which we maximise the related quantity

$$L = \prod_{m=1}^{M} \left(\prod_{t_i \in C_m} \lambda_m(t_i; x) \right) \left(\prod_{t_i \in I} \lambda_m(t_i; x)^{x_{i,m}} \right) e^{-\int_0^T \lambda_m(t;x)dt}$$

[1] The maximand can be replaced with $(\delta + |t_i - t_j|)^{-1}$ if some t_i coincides with some t_j.

where

$$\lambda_m(t;x) = \mu_m + \sum_{t_i \in C_m, t_i < t} g(t - t_i; \theta_m) + \sum_{t_i \in I, t_i < t} x_{i,m} g(t - t_i; \theta_m).$$

If we restrict the vector x_i to be a Kronecker delta, we recover the original maximum likelihood. The relaxation is in the constraint on each x_i: $\|x_i\|_2 = 1$ and $x_{i,m} \geq 0$ for all m. In practice we will maximise not L directly but a quantity that is off by an additive constant from its logarithm, namely

$$F_{\mathrm{MRL}}(x) = \sum_{m=1}^{M} \left(\sum_{t_i \in C_m} \log \lambda_m(t_i;x) + \sum_{t_i \in I} x_{i,m} \log \lambda_m(t_i;x) - \sum_{t_i \in I} x_{i,m} G_m(T - t_i) \right),$$

where $G_m(t) = \int_0^t g(s;\theta_m) ds$. (MRL here stands for *maximum relaxed likelihood*.)

The fourth method is the Stomakhin–Short–Bertozzi (SSB) method outlined in [34]. This essentially maximises F_{SSB} defined by

$$F_{\mathrm{SSB}}(x) = \sum_{m=1}^{M} \sum_{t_i \in I} x_{i,m} \lambda_m(t_i;x)$$

subject to similar constraints on each x_i.

3.2 Numerical implementation

Computing x for the method of modes and nearest-neighbor method is straightforward. Constrained maximisation of F_{SSB} and F_{MRL} requires more care. Both optimisations have the form

$$\boxed{\max F(x) \text{ s.t } \|x_i\|_2 = 1 \,\forall i \text{ and } x_{i,m} \geq 0 \,\forall i, m.}$$

The forms of F are summarised in Table 7. This is a variational approach to the classification problem. Variational methods have had success in various applications, including image processing [3, 4, 32].

Though F_{SSB} was created to approximate the behaviour of F_{MRL}, the two functions have different properties. For example, F_{SSB} is a quadratic function with all positive coefficients, so within the feasible set all its partial derivatives are positive. This means that every component of the maximising x is positive. (See Appendix A for a proof. Briefly, it makes sense to redistribute a little weight from a positive component to a zero component, because the benefit scales linearly with the size of the redistribution, while the cost scales quadratically.) Not so for F_{MRL}:

$$\frac{\partial F_{\mathrm{MRL}}}{\partial x_{i,m}} = \log \lambda_m(t_i;x) + \sum_{t_j \in C_m; t_j > t_i} \frac{g_m(t_j - t_i)}{\lambda_m(t_j;x)} + \sum_{t_j \in I; t_j > t_i} \frac{x_{i,m} g_m(t_j - t_i)}{\lambda_m(t_j;x)} - G_m(T - t_i).$$

The two sums are positive, but the logarithm need not be, and $-G_m(T - t_i)$ can easily be the dominant term.

We used a modified version of the curvilinear search described in [38]. In particular, we can handle inequality constraints, where the original algorithm's constraints are equalities. Also, acknowledging that the gradient may not vanish on our constraint set, we adopt a new stopping criterion. We conclude with some details of our implementation. The whole algorithm appears for reference in Appendix B.

Table 7. *Objective functions*

Method	$F(x)$
SSB	$\sum_{m=1}^{M} \sum_{t_i \in I} x_{i,m} \lambda_m(t_i; x)$
MRL	$\sum_{m=1}^{M} \big(\sum_{t_i \in C_m} \log \lambda_m(t_i; x) + \sum_{t_i \in I} x_{i,m} \log \lambda_m(t_i; x) - \sum_{t_i \in I} x_{i,m} G_m(T - t_i) \big)$

3.2.1 *Wen & Yin's curvilinear search*

Gradient ascent is the most basic and intuitive iterative method for smooth maximisation, but it does not preserve norms. Wen & Yin [38] present a curvilinear adaptation that preserves orthogonal constraints of the form $X^{\mathrm{T}}X = I$, of which our constraint $\|x_i\|_2 = 1$ is a special case. Let $F_{x_i}(x)$ denote the gradient of F with respect to x_i, evaluated at x. Given x and a step size $\tau > 0$, the method computes the update $y_i(\tau, x)$ according to a Crank–Nicolson-type scheme:

$$y_i(\tau, x) = x_i + \tfrac{\tau}{2} A(x, i)(x_i + y_i(\tau, x)),$$

where

$$A(x, i) = F_{x_i}(x) x_i^{\mathrm{T}} - x_i F_{x_i}(x)^{\mathrm{T}}. \tag{3.1}$$

By Lemma 4 in [38], $y_i(\tau, x)$ can be written explicitly as

$$y_i(\tau, x) = (1 - \beta_2) x_i + \beta_1 F_{x_i}(x), \tag{3.2}$$

where

$$\begin{aligned} \beta_1 &= \frac{\tau}{1 + (\frac{\tau}{2})^2 \delta_i(x))}, \\ \beta_2 &= (F_{x_i}(x)^{\mathrm{T}} x_i + \tfrac{\tau}{2} \delta_i(x)) \beta_1, \\ \delta_i(x) &= \|F_{x_i}(x)\|_2^2 - (F_{x_i}(x)^{\mathrm{T}} x_i)^2. \end{aligned}$$

Because $\|x_i\|_2 = 1$, the Cauchy–Schwarz inequality ensures that $\delta_i(x) \geq 0$. Furthermore, $\frac{d}{d\tau} F(y(\tau, x))|_{\tau=0} = \frac{1}{2}\delta_i(x)$, so $y_i(\tau, x)$ is an ascent direction.

Classical Crank–Nicolson would use $\frac{1}{2}(F_{x_i}(x) + F_{x_i}(y(\tau, x)))$ as the step direction, where $y(\tau, x)$ is x but with $y_i(\tau, x)$ replacing x_i. However, this does not guarantee the spherical constraint. By contrast a straightforward calculation verifies that if $\|x_i\|_2 = 1$, then $\|y_i(\tau, x)\|_2 = 1$ for all $\tau > 0$. The form of A (3.1) is inspired by work on p-harmonic flows with spherical constraints [12, 37].

3.2.2 *Inequality constraints*

The algorithm in [38] simply sets $x_i^{(k+1)} = y_i(\tau, x_i^{(k)})$, with some adaptive time stepping for τ. While this preserves $\|x_i\|_2$, it does not preserve the signs of the components of x_i. Our family of inequality constraints ($x_{i,m} \geq 0$ for each i and each m) forces us to concern ourselves with the signs, altering the problem fundamentally.

If each component of $x^{(k)}$ (the k^{th} iterate) is positive but some component of $y_i(\tau, x_i^{(k)})$ is negative, then there exists a largest $\sigma \in (0, \tau)$ so that $y_i(\sigma, x^{(k)})$ has all non-negative components. This σ is actually straightforward to compute, because each equation of

the form $y_{i,m}(\sigma, x_i^{(k)}) = 0$ is quadratic in σ. However, we found that this technique was slow in practice because it only allows one dimension of x_i to reach 0 at a time. When $F = F_{\mathrm{SSB}}$, many components of the maximiser x_i^* are close to 0, so we would like to allow many of them to reach 0 at once so they can then turn around and find their correct (small, positive) value. When $F = F_{\mathrm{MRL}}$, many dimensions will ultimately belong to the active set, and we would like to identify several of them at a time if possible. Therefore, we adopt the less elegant but faster method of setting $z = \max(0, y_i(\tau, x_i^{(k)}))$, with the max done componentwise, and then redistributing the mass to preserve the ℓ^2 norm, i.e. $\tilde{x}_i^{(k+1)} = z/\|z\|_2$.

If we adopt $x_i^{(k+1)} = \tilde{x}_i^{(k+1)}$, then it may have components that are zero and that will become negative after another iteration of the curvilinear search. If we continue with these components, the algorithm may hang because the projection back to the sphere may become parallel to the curvilinear search direction. We can prevent this if we acknowledge that any dimensions m for which $y_{i,m}(\tau, \tilde{x}_i^{(k+1)}) < 0$ belong to the active set of inequality constraints. Noting from (3.2) that $y_{i,m}(\tau, x)$ and $F_{x_i}(x)$ have the same sign when $x_{i,m} = 0$, we set $x_i^{(k+1)} = P(x, \tilde{x}_i^{(k+1)})\tilde{x}_i^{(k+1)}$, where $P(x, \tilde{x}_i^{(k+1)})$ is the projection onto the subspace of those dimensions m for which $\tilde{x}_{i,m}^{(k+1)} > 0$ or $F_{x_i} > 0$, with the derivative evaluated at x except with x_i replaced with $\tilde{x}_i^{(k+1)}$. (As we iterate, we also remove dimensions from F and ∇F so that dot products with x_i still make sense and so that we are not calculating derivatives unnecessarily.)

When $F = F_{\mathrm{SSB}}$ the solution can have many small positive components. It is possible that at $x_i^{(1)}$ many components $x_{i,m}^{(1)}$ are small and positive but have $y_{i,m}(\tau, x^{(1)}) < 0$, and many others are zero but have $y_{i,m}(\tau, x^{(1)}) > 0$. These sets of components trade places in $x_i^{(2)}$, and the next iteration will send it back to very close to $x_i^{(1)}$. If enough components keep "trading places" like this it can cause the algorithm to hang without reaching the stopping criterion. We found that when $|I|$ was large this happened a small but nontrivial percentage of the time. We also found that we could eliminate the problem by checking the signs of the components of x_i versus $y_i(\tau, x)$. If most were different, we tried $y_i(\tau/2, x)$, and then $y_i(\tau/4, x)$, and so on until a majority of the signs were preserved.

Once the iteration completes, we need to check that the dimensions we have projected away still correspond to active constraints. If they do not, we project $x^{(k)}$ into a larger space including the inactivated dimensions and resume iterating.

3.2.3 *Stopping criterion*

Wen & Yin [38] give a stopping criterion of $\|\nabla F\|_2 < \epsilon$. Our stopping criterion must be different, because we do not expect $\|\nabla F\|_2$ to decrease to 0 as we iterate. (Indeed, as noted above, the components of ∇F_{SSB} are always positive.) Instead we look for ∇F to be normal to the constraint surface. Since the constraint surface is a sphere, this means we want $\nabla F \cdot x$ to be large relative to the size of ∇F. Specifically, our stopping criterion is

$$\min_{t_i \in I} \frac{|F_{x_i}(x_i^{(k)}) \cdot x_i^{(k)}|}{\|F_{x_i}(x_i^{(k)})\|_2} > 1 - \epsilon.$$

The absolute value in the numerator is necessary only if every $F_{x_i}(x_i^{(k)})$ is negative. This can happen when $F = F_{\mathrm{MRL}}$ but not when $F = F_{\mathrm{SSB}}$.

3.2.4 *Practical computing considerations*

The most computationally expensive part of our C++ implementation of the algorithm is the computation of the derivative F_{x_i}. Care must be taken to minimise this expense. For reference, its components for our two choices of F are

$$\frac{\partial F_{\mathrm{SSB}}}{\partial x_{i,m}} = \mu_m + \sum_{t_j \in C_m} g_m(|t_i - t_j|) + \sum_{t_j \in I;\, t_j \neq t_i} x_{j,m} g_m(|t_i - t_j|), \tag{3.3}$$

and

$$\frac{\partial F_{\mathrm{MRL}}}{\partial x_{i,m}} = \log \lambda_m(t_i; x) + \sum_{t_j \in C_m;\, t_j > t_i} \frac{g_m(t_j - t_i)}{\lambda_m(t_j; x)} + \sum_{t_j \in I;\, t_j > t_i} \frac{x_{i,m} g_m(t_j - t_i)}{\lambda_m(t_j; x)} - G_m(T - t_i).$$

Values of g_m should never be computed "on the fly"; each should be precomputed and stored. Most of these values will be so small that treating them as zero will have a *de minimis* impact on the results, but avoiding computing them (and computing with them) saves tremendous time. Set a small threshold $\eta > 0$, and compute $g_m(t_i - t_j)$ only if it will exceed $\eta\mu_m/|C_m|$, i.e. if $|t_i - t_j| < g_m^{-1}(\eta\mu_m/|C_m|)$. This adds a layer of dependency tracking, but the savings in floating point operations are well worth it.

When $F = F_{\mathrm{SSB}}$, the update formula

$$\frac{\partial F_{\mathrm{SSB}}}{\partial x_{i,m}}(x^{(1)}) = \frac{\partial F_{\mathrm{SSB}}}{\partial x_{i,m}}(x^{(0)}) + \sum_{t_j \in I;\, t_j \neq t_i} g_m(|t_i - t_j|)(x_{j,m}^{(1)} - x_{j,m}^{(0)})$$

can save time when recomputing F_{x_i}. When $F = F_{\mathrm{MRL}}$, a corresponding update formula applies for $\lambda_m(t_j; x)$. The λ values should be tracked, while the logarithm should be computed only when it is needed.

4 Results

Here we present results for different configurations of missing data. First we present results from the IkeNet data set. Then we test the methods on simulated point patterns on artificial social networks, including some toy networks and some meant to resemble IkeNet. We conclude the section by discussing the results in detail.

In each of our tests we begin with a complete data set, whether it is real (IkeNet) or simulated. Then we knock out some of the information to see whether we can recover it from the rest of the corpus. The information might be a particular email's sender or receiver, an email's sender *and* receiver, or the senders and receivers of several emails. When deleting one record at a time we repeat this for each record in the corpus. When deleting more than one record, exhausting the space of combinations is infeasible, so we take a Monte Carlo approach.

We consider a data recovery method successful when the correct component $x_{i,m}$ has a high weight relative to other components. In particular, we want $x_{i,m}$ to be the greatest

Table 8. *IkeNet: Predictive power for missing sender by method ($|I| = 1$)*

Method	Top 1	Top 2	Top 3	Top 5	Top 10
Modes	27.8%	41.1%	50.0%	62.9%	82.0%
NN	62.9%	75.1%	79.8%	85.3%	92.6%
SSB	63.1%	74.7%	80.0%	85.8%	93.3%
MRL	61.1%	70.0%	72.4%	73.3%	73.6%

Table 9. *IkeNet: Predictive power for missing receiver by method ($|I| = 1$)*

Method	Top 1	Top 2	Top 3	Top 5	Top 10
Modes	30.4%	43.5%	52.1%	64.4%	82.7%
NN	58.0%	73.3%	80.1%	86.6%	93.9%
SSB	59.2%	73.9%	80.6%	87.1%	93.7%
MRL	58.9%	69.0%	71.7%	72.6%	72.8%

component, or perhaps the second or third greatest. This metric was considered previously in [34] based on input from the LAPD. (The context there was solving gang crimes, where narrowing down the list of suspect gangs to three can help detectives.) We also present the results for top 5 and top 10 to showcase a property of the MRL optimiser.

We estimate the Hawkes process parameters using the techniques described in section 2. The SSB and MRL iterations are seeded with the solution from the nearest-neighbor method.

4.1 IkeNet

4.1.1 *Unidirectional identity loss, one at a time*

First we took each email in the corpus and saw whether we could determine who sent it knowing its receiver and the rest of the corpus. Repeating this for each email in the corpus meant 8,896 separate runs with $|I| = 1$ each time. The average performance is shown in Table 8.

Table 8 shows that SSB, nearest-neighbor (NN), and MRL guess the correct sender about 60% of the time. There is a clear ranking among them, with SSB outperforming nearest-neighbor and nearest-neighbor outperforming MRL. MRL's relative performance decreases left to right. The method of modes performs poorer than the other methods.

Table 9 shows the results when we repeat the process but try to guess the receiver knowing the sender. The numbers are slightly different, but the same patterns prevail.

4.1.2 *Unidirectional identity loss, missing proportions*

We now consider what happens when larger blocks of data are missing, which will be the case in applications. We selected a percentage of the emails at random and removed the sender or receiver information (chosen randomly for each email). We then attempted to

Table 10. *IkeNet: Predictive power for unidirectional identity loss ($|I| > 1$)*

$\|I\|/N$	Method	Top 1	Top 2	Top 3	Top 5	Top 10
5%	Modes	29.1%	42.2%	50.9%	63.1%	82.1%
	NN	59.9%	73.5%	79.3%	85.4%	93.0%
	SSB	59.9%	73.5%	79.7%	86.0%	93.3%
	MRL	59.4%	68.9%	71.4%	72.2%	72.4%
10%	Modes	29.1%	42.2%	50.9%	63.1%	82.1%
	NN	59.3%	72.8%	78.6%	84.7%	92.6%
	SSB	58.8%	72.7%	79.0%	85.5%	93.1%
	MRL	58.9%	68.3%	70.7%	71.5%	71.7%
15%	Modes	29.1%	42.1%	50.9%	63.1%	82.1%
	NN	58.7%	72.1%	77.8%	84.1%	92.3%
	SSB	57.7%	71.9%	78.4%	85.1%	92.9%
	MRL	58.3%	67.6%	69.9%	70.7%	70.8%
20%	Modes	29.1%	42.1%	50.9%	63.1%	82.0%
	NN	58.0%	71.2%	77.0%	83.4%	91.9%
	SSB	56.7%	71.1%	77.7%	84.6%	92.6%
	MRL	57.7%	66.8%	69.1%	69.9%	70.0%

recover the missing data. We repeated this process for 10,000 Monte Carlo runs at each missing percentage.

Table 10 shows the results. As expected, the performance decreases as the missing proportion increases from 5% to 20%, but only by a few percentage points. This demonstrates the methods' robustness to larger missing blocks of data. Interestingly, MRL overtakes SSB as the missing proportion increases, but only for top 1. The method of modes experiences no degradation. This is not a surprise; it returns the same top pairs shown in Table 1 until enough data is missing in the right places that the order statistics change.

4.1.3 *Bidirectional identity loss, one at a time*

We repeated the one-at-a-time procedure with deleting both sender and receiver from each email, resulting in *bidirectional identity loss*. Table 11 presents the results. The methods do not perform as well as when only the sender or receiver is missing because instead of choosing among the 22 edges connected to each nodes they must choose among the 253 edges in the complete graph.[2] Nonetheless the local methods guessed the correct edge about 40% of the time and got in the top 3 about 55-60% of the time. MRL still underperforms, but by less than with unidirectional loss. The method of modes continues to underperform all other methods.

Table 12 presents average numerical values of F_{SSB} and F_{MRL} evaluated at the bidi-

[2] Actually there are only 250 edges; as noted above, three pairs of agents exchanged no emails.

Table 11. *IkeNet: Predictive power for bidirectional identity loss ($|I| = 1$)*

Method	Top 1	Top 2	Top 3	Top 5	Top 10
Modes	11.7%	17.5%	20.9%	27.3%	36.7%
NN	37.9%	51.3%	58.5%	65.6%	73.2%
SSB	39.6%	51.1%	57.6%	65.3%	73.0%
MRL	36.4%	47.8%	55.0%	61.4%	66.1%

Table 12. *IkeNet: Average energy values for bidirectional identity loss ($|I| = 1$)*

Method	F_{SSB}	F_{MRL}
Modes	45.82	85.62
NN	122.39	99.37
SSB	141.39	99.47
MRL	118.09	101.01

Table 13. *IkeNet: Predictive power for bidirectional identity loss ($|I| > 1$)*

$\|I\|/N$	Method	Top 1	Top 2	Top 3	Top 5	Top 10
5%	Modes	11.7%	17.5%	20.8%	27.3%	36.7%
	NN	37.6%	50.8%	57.9%	64.9%	72.4%
	SSB	38.6%	50.4%	56.9%	64.3%	72.2%
	MRL	36.0%	47.4%	54.4%	60.9%	65.2%
10%	Modes	11.7%	17.5%	20.8%	27.3%	36.7%
	NN	37.3%	50.3%	57.2%	64.1%	71.5%
	SSB	37.5%	49.3%	55.8%	63.2%	71.3%
	MRL	35.6%	47.0%	53.8%	60.2%	64.4%

rectional identity loss solutions in Table 11.[3] Horizontal comparison of the values is meaningless, but vertical comparison is not. The results verify that the SSB and MRL solutions maximise F_{SSB} and F_{MRL}, respectively.

4.1.4 *Bidirectional identity loss, missing proportions*

Table 13 shows the results of the Monte Carlo approach for larger blocks of missing bidirectional data. Bidirectional is much more intensive computationally than unidirectional, so we present proportions only up to 10% here. The degradation is again modest (compare with Table 11), and the ranking of methods is consistent.

Table 14 shows average energy values, normalised by the size of the missing block for comparison with Table 12. The values are close, and the same hierarchies are apparent.

[3] The values in Table 12 are actually of $F(x) - F_{\min}$ to highlight the differences in scale.

Table 14. *IkeNet: Average energy values for bidirectional identity loss ($|I|/N = 5\%$)*

Method	$F_{\mathrm{SSB}}/\lvert I\rvert$	$F_{\mathrm{MRL}}/\lvert I\rvert$
Modes	49.12	84.08
NN	120.67	97.87
SSB	147.45	97.88
MRL	115.53	100.12

4.2 Simulated point patterns

We simulate Hawkes processes on two classes of networks. First we consider some toy networks with simple structures. Then we simulate a faux IkeNet (*FauxNet*) using the IkeNet parameters.

4.2.1 *Toy networks*

We use three different configurations of toy networks. Like IkeNet they have 22 nodes, but a known interaction structure. We assume that g is exponential with $\alpha = 0.5$, $\omega = 6$, with the background rate μ varying to show different levels of interaction.

- *Dense*: All nodes are connected to each other (a complete graph), with a low rate of interaction ($\mu = 0.03$).
- *Sparse*: The nodes are arranged in a ring. Each node is connected to its two neighbors and to the node opposite it in the ring, so that the graph looks like a wheel with spokes (except there is no node at the axle). Interaction rates between connected nodes are high ($\mu = 0.1$). Unconnected nodes do not interact.
- *Pseudosparse*: A complete graph, with high interaction ($\mu = 0.1$) between the nodes connected in the sparse graph and low interaction ($\mu = 0.03$) between other pairs.

Table 15 presents the results for Monte Carlo simulation. For each network, we adopted bidirectional identity loss for each record in succession, and then averaged the results over each Monte Carlo simulation. Table 15 compares with Table 11.

The method of modes performs very poorly here compared with IkeNet, because the toy networks lack the heterogeneity in activity levels evident in Table 1 and Figure 3. NN, SSB, and MRL perform similarly, as with IkeNet, but here MRL outperforms NN. SSB still outperforms them both. Unsurprisingly, all methods perform better on the sparse network than on the dense network, but the local methods perform very well compared to the method of modes even on the dense network. Interestingly, though the performance of the method of modes on the pseudosparse network is between its performances on the dense and sparse networks, the local methods perform worst on the pseudosparse network. This is because the local methods perform poorer as the number of pairs experiencing a burst of activity at any given time increases. This strength of this effect decreases as we move from top 1 to top 10, and indeed this is reflected in Table 15.

Table 15. *Toy networks: Predictive power for bidirectional identity loss ($|I| = 1$)*

Network	Method	Top 1	Top 2	Top 3	Top 5	Top 10
Dense	Modes	1.0%	1.9%	2.7%	4.3%	7.9%
	NN	21.4%	36.5%	47.0%	59.3%	69.0%
	SSB	27.4%	41.6%	50.6%	61.0%	69.7%
	MRL	26.4%	40.9%	49.6%	57.9%	61.9%
Sparse	Modes	4.5%	8.6%	12.4%	20.1%	37.7%
	NN	36.9%	55.5%	65.0%	72.6%	78.8%
	SSB	40.8%	57.5%	65.8%	73.0%	79.6%
	MRL	39.8%	55.9%	62.0%	63.6%	64.9%
Pseudosparse	Modes	1.5%	2.8%	4.2%	6.7%	12.5%
	NN	17.9%	31.4%	41.5%	54.7%	67.6%
	SSB	23.7%	36.8%	45.8%	57.0%	68.3%
	MRL	23.0%	36.2%	45.1%	54.9%	61.5%

Table 16. *FauxNet: Predictive power for bidirectional identity loss ($|I| = 1$)*

Method	Top 1	Top 2	Top 3	Top 5	Top 10
Modes	11.7%	17.5%	21.1%	27.5%	37.0%
NN	49.4%	60.2%	63.9%	66.8%	70.3%
SSB	53.6%	63.2%	66.8%	70.1%	74.3%
MRL	48.5%	60.6%	64.5%	65.9%	66.0%

Table 17. *FauxNet: Predictive power for bidirectional identity loss ($|I|/N = 5\%$)*

Method	Top 1	Top 2	Top 3	Top 5	Top 10
Modes	11.7%	17.4%	21.0%	27.3%	36.8%
NN	48.9%	59.4%	63.0%	66.0%	69.4%
SSB	52.4%	62.0%	65.7%	69.1%	73.4%
MRL	47.9%	59.8%	63.6%	65.0%	65.1%

4.2.2 *FauxNet*

As with the toy networks, we took a Monte Carlo approach to FauxNet, the simulated IkeNet, and present results for bidirectional identity loss in Tables 16 and 17. The method of modes performs almost the same as in IkeNet (see Tables 11 and 13). The other methods perform better here by several percentage points.

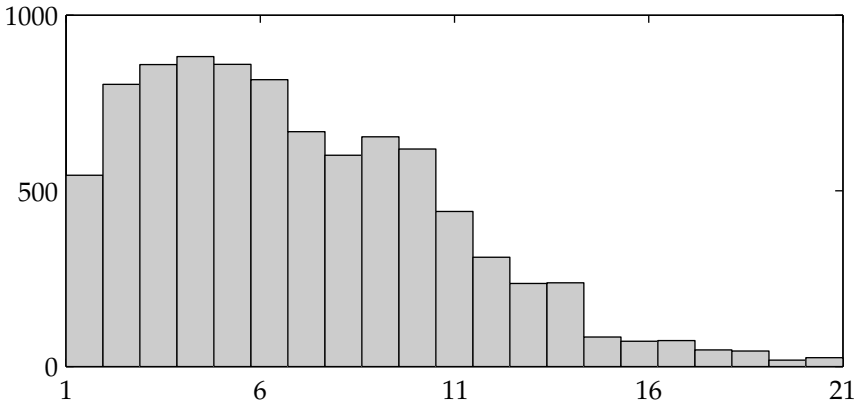

FIGURE 6. Histogram of $\|x_{\mathrm{MRL}}\|_0$ for bidirectional identity loss, $|I| = 1$, for all 8,896 cases.

4.3 Discussion

In all our results, the local methods (nearest-neighbor, SSB, and MRL) strongly outperform the purely global method of modes. This suggests that most of the information in these sorts of records is local. Meanwhile, with IkeNet the model-free nearest-neighbor method performs comparably to the variational methods (SSB and MRL) developed in section 3. With the simulated Hawkes process data it underperforms SSB and, in some places, MRL, but not by nearly the margin that the method of modes does. This suggests that the Hawkes process is an imperfect model for real human communication like the IkeNet data, but the loss incurred from these assumptions is modest. On the other hand, the loss in assuming no model at all (i.e. using nearest-neighbor) is also modest and has the virtue of being simpler to implement, understand, and communicate outside technical literature.

The improvement in MRL's performance as it moves from top 5 to top 10 is considerably lower than it is for the other methods. Figure 6 reveals why. It shows a histogram of $\|x_{\mathrm{MRL}}\|_0$, the number of nonzero components of x_{MRL}, for each bidirectional $|I| = 1$ case. The median is 6, and $\|x_{\mathrm{MRL}}\|_0 \leq 5$ in about 44% of cases. In these cases, if the correct pair is not in the top 5 then it will not be in the top 10, either. SSB, by contrast, always has full ℓ^0 norm (see Appendix A for a proof), and even if the correct pair has only a small positive weight it is often larger enough than the other small positive weights to make it to the top 10. Of course, MRL has even fewer positive components in the unidirectional case, explaining why it underperforms less in bidirectional identity loss. Thus SSB's density is capturing some faint information that MRL misses by being so sparse. If a likelihood approach like MRL is to beat SSB it will likely have to mimic this ability.

All the methods except the method of modes perform better on FauxNet than on IkeNet. Furthermore, SSB and MRL perform better relative to nearest-neighbor on the simulated point patterns than they do on IkeNet data. Both these observations suggest that the Hawkes process is an imperfect model for the behaviour driving IkeNet.

5 Conclusion

We demonstrated that, when estimating the parameters of a Hawkes process from the IkeNet data, choosing a parameterisation for the triggering function is less important than using the correct values of the parameters. We then developed a method for filling in missing data for interactions within social networks and presented some results from the IkeNet data set. The method's power even when the proportion of missing data increases has implications for security, surveillance, and privacy. In particular, it suggests that access to even a fraction of a complete record can reveal a great deal of information about the remainder, emphasising the need for robust access controls.

Future work should address how network structure impacts the ability to fill in missing data. Exogenous information (for example, the leadership relationships among the IkeNet officers) may also be able to boost the method's power. Future work might also seek an objective function combining MRL's fidelity to the original likelihood with SSB's solution density.

This work also leaves open several interesting avenues for research on self-exciting point processes. To the extent that our finding on the impact of model selection vs. parameter selection can be extended to other model classes and parameter regimes, it will justify the common practice of assuming an exponential form for the triggering function without a specific justification for the choice. However, as noted, modelling IkeNet's email behaviours with Hawkes processes has its limits, so consideration of other classes of self-exciting point processes for this and other human communication data sets may be warranted.

Acknowledgements

This research was supported by NSF grants DMS-0968309, DMS-1118971, and DMS-1417674, AFOSR MURI grant FA 9550-10-1-0569, ONR grant N000141210838, ARO MURI grant W911NF-11-1-0332, and ARI MIPR 10086985. When this work was performed the first author was supported by a National Defense Science and Engineering Graduate (NDSEG) Fellowship. We thank Eric Fox, Martin Short, Alexey Stomakhin, and Wotao Yin for helpful discussions, and U.S. Army Maj. Ian McCulloh for coordinating data collection.

Appendix A Geometry of SSB maximisation

We prove that the SSB weight vector always has all positive components, as a corollary of the following. Intuitively, it makes sense to redistribute a little weight from a positive component to a zero component, because the benefit scales linearly with the size of the redistribution, while the cost scales quadratically.

Proposition *Let $n \geq 2$, and let D be the portion of the unit sphere in the non-negative orthant of R^n, i.e. $D = \{x \in \mathsf{R}^n : \|x\|_2 = 1, x_i \geq 0 \, \forall i\}$. Let $f : \mathsf{R}^n \to \mathsf{R}$ be differentiable with all positive partial derivatives on the non-negative orthant. Then there exists $x^* \in D$ maximising f on D, and $\|x^*\|_0 = n$, i.e. every component of x^* is nonzero.*

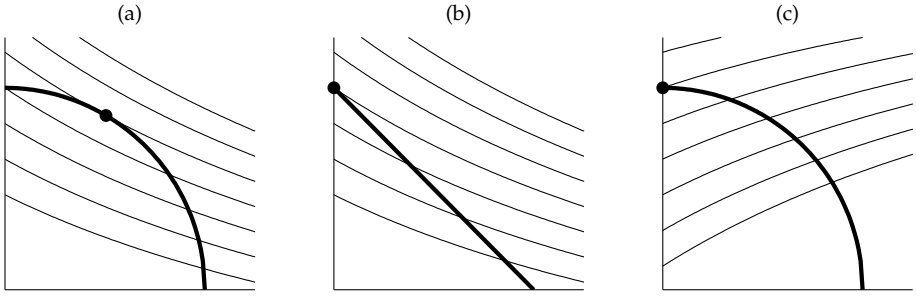

FIGURE A 1. Diagrams of ℓ^p constraints (bold) with level sets of a function f. The dot indicates the point maximising f subject to the constraint. It occurs at the intersection between the constraint and the maximal level set that intersects it. (a) $p = 2$, $\partial f/\partial x_1 > 0$, $\partial f/\partial x_2 > 0$. (b) $p = 1$, $\partial f/\partial x_1 > 0$, $\partial f/\partial x_2 > 0$. (c) $p = 2$, $\partial f/\partial x_1 < 0$, $\partial f/\partial x_2 > 0$.

Proof x^* exists because f is continuous and D is compact. Suppose by way of contradiction that $\|x^*\|_0 < n$. Without loss of generality, $x_1^* = 0$. By assumption $\|x^*\|_2 = 1$, so without loss of generality $x_2^* > 0$. Define $\xi : [0, x_2^*] \to \mathsf{R}^n$ by

$$\xi_i(t) = \begin{cases} t & \text{if } i = 1, \\ \sqrt{(x_2^*)^2 - t^2} & \text{if } i = 2, \\ x_i^* & \text{if } 3 \leq i \leq n. \end{cases}$$

Then $\xi(t) \in D$ for every t. Because f is differentiable there exist $t_0 > 0$ and $h : (0, t_0) \to \mathsf{R}$ such that $h(t) = o(t)$ as $t \to 0$, and if $0 < t < t_0$ then

$$f(\xi(t)) = f(x^*) + t\nabla f(x^*)^{\mathrm{T}}\xi'(0) + h(t).$$

Easy computations show that $\xi_1'(0) = 1$, $\xi_2'(0) = 0$, and $\xi_i'(0) = 0$ if $3 \leq i \leq n$, so

$$f(\xi(t)) = f(x^*) + t\frac{\partial f}{\partial x_1}(x^*) + h(t).$$

By assumption $\frac{\partial f}{\partial x_1}(x^*) > 0$, so there exists $t_1 \in (0, t_0]$ such that if $0 < t < t_1$ then $|h(t)|/t < \frac{1}{2}\frac{\partial f}{\partial x_1}(x^*)$, in which case

$$f(\xi(t)) > f(x^*) + t\frac{\partial f}{\partial x_1}(x^*) - \frac{t}{2}\frac{\partial f}{\partial x_1}(x^*) > f(x^*),$$

contradicting the assumption that x^* maximises f on D. Thus in fact $\|x^*\|_0 = n$. □

This result recalls a familiar observation about the geometry of ℓ^2 optimisation, presented in two dimensions in Figure A 1. When all partial derivatives are positive, the geometry is as in Figure A 1(a). If at some point a level set lies tangent to the constraint, or equivalently the gradient is normal to the constraint, then this point is an optimiser. (This is the basis for the theory of Lagrange multipliers.) The partial derivatives are positive, so the level sets have negative slope. In the non-negative quadrant the ℓ^2 constraint takes every negative number as a slope, so a point of tangency is guaranteed to exist. This is often contrasted with the ℓ^1 case, where the constraint takes only one slope

and tangency may not occur, as in Figure A 1(b). (This is why ℓ^1 optimisers are often sparse, for example as in [2, 8, 9, 32].) However, one can just as easily contrast Figure A 1(a) with Figure A 1(c), where the negative sign of one of the partial derivatives produces positively sloped level sets. Because we are not permitted outside the non-negative orthant, we must settle for the solution on the boundary. Figure A 1(a) corresponds to F_{SSB}, and Figure A 1(c) corresponds to F_{MRL}.

Nonetheless, the assumptions that all partial derivatives of f on the non-negative orthant be positive was stronger than necessary. It would have sufficed if, for every $y \in D$ with a zero component $y_i = 0$, $\frac{\partial f}{\partial x_i}(y) > 0$. However, it is clear from (3.3) that F_{SSB} satisfies the stronger assumption stated in the proposition except in the trivial, degenerative case when some $\mu_m = 0$.

Appendix B Curvilinear search algorithm

while $\max_{t_i \in I} |F_{x_i}(x_i) \cdot x_i| / \|F_{x_i}(x_i)\|_2 > \epsilon$ **do**
  for $i = 1 : |I|$ **do**
    $v = F_{x_i}(x)$
    $\delta = \|v\|_2^2 - (v^{\mathrm{T}} x_i)^2$
    $\beta_1 = \tau / (1 + (\frac{\tau}{2})^2 \delta)$
    $\beta_2 = (v^{\mathrm{T}} x_i + \frac{\tau}{2}\delta)\beta_1$
    $y = (1 - \beta_2) x_i + \beta_1 F_{x_i}(x)$
    $\overline{\tau} = \tau$
    while most components of y have different signs than x_i **do**
      $\overline{\tau} = \overline{\tau}/2$
      $\beta_1 = \overline{\tau} / (1 + (\frac{\overline{\tau}}{2})^2 \delta)$
      $\beta_2 = (v^{\mathrm{T}} x_i + \frac{\overline{\tau}}{2}\delta)\beta_1$
      $y = (1 - \beta_2) x_i + \beta_1 F_{x_i}(x)$
    end while
    $z = \max(0, y)$ componentwise
    $\tilde{x} = x$
    $\tilde{x}_i = z / \|z\|_2$
    $v = F_{x_i}(\tilde{x})$
    Let P project the space of x_i to the subspace where $\tilde{x}_{i,m} > 0$ or $v_m > 0$
    $x_i = P \tilde{x}_i$
    $F_{x_i} = P F_{x_i}$
  end for
end while
for $i = 1 : |I|$ **do**
  Let Q project the space of x_i into its original, full space
  $w_i = Q x_i$
  $F_{x_i} = Q F_{x_i}$
end for
startover = false
for $i = 1 : |I|$ **do**
  $v = F_{x_i}(w)$

```
    for all m in the space of w_i do
        if m is not in the space of x_i and v_i > 0 then
            Project x_i into its own space augmented with dimension m
            startover = true
        end if
    end for
end for
if startover then
    for i = 1 : |I| do
        Project F_{x_i} into the space of x_i
    end for
    Return to the start
end if
```

References

[1] Barabási, A.-L. 2005 The origin of bursts and heavy tails in human dynamics. *Nature* **435**, 207–11.

[2] Candès, E. J., Romberg, J. K. & Tao, T. 2006 Stable signal recovery from incomplete and inaccurate measurements. *Communications on Pure and Applied Mathematics* **59**, 1207–23.

[3] Chambolle, A., Caselles, V., Cremers, D., Novaga, M. & Pock, T. 2010 An introduction to total variation for image analysis. In Fornasier, Massimo, ed. 2010 *Theoretical foundations and numerical methods for sparse recovery*. Berlin. De Gruyter, 263–340.

[4] Chan, T. F. & Shen, J. 2005 *Image processing and analysis: variational, PDE, wavelet, and stochastic methods*. Philadelphia. SIAM.

[5] Cho, Y. S., Galstyan, A., Brantingham, P. J. & Tita, G. 2014 Latent self-exciting point process model for spatial-temporal networks. *Discrete and Continuous Dynamical Systems B* **19**, 1335–54.

[6] Crane, R. & Sornette, D. 2008 Robust dynamic classes revealed by measuring the response function of a social system. *Proceedings of the National Academy of Sciences* **105**, 15649–53.

[7] Csermely, P., London, A., Wu, L.-Y., & Uzzi, B. 2013 Structure and dynamics of core/periphery networks. *Journal of Complex Networks* **1**, 93–123.

[8] Donoho, D. L. 2006 Compressed sensing. *IEEE Transactions on Information Theory* **52**, 1289–1306.

[9] Donoho, D. L. & Tanner, J. 2005 Sparse nonnegative solution of underdetermined linear equations by linear programming. *Proceedings of the National Academy of Sciences* **102**, 9446–51.

[10] Egesdal, M., Fathauer, C., Louie, K., Neuman, J., Mohler, G. & Lewis, E. 2010 Statistical modeling of gang violence in Los Angeles. *SIAM Undergraduate Research*.

[11] Fox, E. W., Short, M. B., Schoenberg, F. P., Coronges, K. D. & Bertozzi, A. L. 2014 Modeling e-mail networks and inferring leadership using self-exciting point processes. Submitted to *Journal of the American Statistical Association*.

[12] Goldfarb, D., Wen, Z. & Yin, W. 2009 A curvilinear search method for p-harmonic flows on spheres. *SIAM Journal on Imaging Sciences* **2**, 84–109.

[13] Hawkes, A. G. 1971 Spectra of self-exciting and mutually exciting point processes. *Biometrika* **58**, 83–90.

[14] —. 1971 Point spectra of some mutually exciting point processes. *Journal of the Royal Statistical Society B* **33**, 438–43.

[15] Hegemann, R. A., Lewis, E. A., & Bertozzi, A. L. 2013 An "Estimate & Score Algorithm" for simultaneous parameter estimation and reconstruction of incomplete data on social networks. *Security Informatics* **2**, 1.

[16] Isella, L., Stehlé, J., Barrat, A., Cattuto, C., Pinton, J.-F. & Van den Broeck, W. 2011 What's in a crowd? Analysis of face-to-face behavioral networks. *Journal of Theoretical Biology* **271**, 166–80.

[17] Lee, N. H., Yoder, J., Tang, M. & Priebe, C. E. 2013 On latent position inference from doubly stochastic messaging activities. *Multiscale Modeling and Simulation* **11**, 683–718.

[18] Lewis, E., & Mohler, G. 2011 A nonparametric EM algorithm for multiscale Hawkes processes. Preprint.

[19] Lewis, E., Mohler, G., Brantingham, P. J., & Bertozzi, A. 2010 Self-exciting point process models of insurgency in Iraq. UCLA CAM Report 10-38.

[20] Lewis, P. A. W. & Shedler, G. S. 1979 Simulation of nonhomogeneous Poisson processes by thinning. *Naval Research Logistics Quarterly* **26**, 403–13.

[21] Marsan, D. & Lengliné, O. 2008 Extending earthquakes' reach through cascading. *Science* **319**, 1076–79.

[22] Masuda, N., Takaguchi, T., Sato, N. & Yano, K. 2013 Self-exciting point process modeling of conversation event sequences. In Holme, P. & Saramäki, J., eds. 2013 *Temporal networks*. Berlin. Springer–Verlag, 245–64.

[23] McLachlan, G. J. & Krishnan, T. 2008 *The EM algorithm and extensions* (2nd edn). Hoboken, New Jersey. Wiley.

[24] Miritello, G., Moro, E., & Lara, R. 2011 Dynamical strength of social ties in information spreading. *Physical Review E* **83**, 045102(R).

[25] Mohler, G. 2013 Modeling and estimation of multi-source clustering in crime and security data. *Annals of Applied Statistics* **7**, 1525–39.

[26] Ogata, Y. 1981 On Lewis' simulation method for point processes. *IEEE Transactions on Information Theory* **27**, 23–31.

[27] — 1998 Space-time point process models for earthquake occurrences. *Annals of the Institute of Statistical Mathematics* **50**, 379–402.

[28] — 1999 Seismicity analysis through point-process modeling: a review. *Pure and Applied Geophysics* **155**, 471–501.

[29] Ozaki, T. 1979 Maximum likelihood estimation of Hawkes' self-exciting point processes. *Annals of the Institute of Statistical Mathematics* **31**, 145–55.

[30] Paxson, V. & Floyd, S. 1995 Wide area traffic: the failure of Poisson modeling. *IEEE/ACM Transactions on Networking* **3**, 226–44.

[31] Rubin, I. 1972 Regular point processes and their detection. *IEEE Transactions on Information Theory* **18**, 547–57.

[32] Rudin, L. I., Osher, S., & Fatemi, E. 1992 Nonlinear total variation based noise removal algorithms. *Physica D* **60**, 259–68.

[33] Rybski, D., Buldyrev, S. V., Havlin, S., Liljeros, F., & Makse, H. A. 2009 Scaling laws of human interaction activity. *Proceedings of the National Academy of Sciences* **106**, 12640–45.

[34] Stomakhin, A., Short, M. B. & Bertozzi, A. L. 2011 Reconstruction of missing data in social networks based on temporal patterns of interactions. *Inverse Problems* **27**, 115013.

[35] Vázquez, A., Oliveira, J. G., Dezsö, Z., Goh, K.-I., Kondor, I., & Barabási, A.-L. 2006 Modeling bursts and heavy tails in human dynamics. *Physical Review E* **73**, 036127.

[36] Veen, A. & Schoenberg, F. P. 2008 Estimation of space–time branching process models in seismology using an EM-type algorithm. *Journal of the American Statistical Association* **103**, 614–24.

[37] Vese, L. A. & Osher, S. J. 2002 Numerical methods for p-harmonic flows and applications to image processing. *SIAM Journal on Numerical Analysis* **40**, 2085–2104.

[38] Wen, Z. & Yin, W. 2013 A feasible method for optimization with orthogonality constraints. *Mathematical Programming A* **142**, 397–434.

[39] Wu, C. F. J. 1983 On the convergence properties of the EM algorithm. *Annals of Statistics* **11**, 95–103.